Grating theory: new equations in Fourier space leading to fast converging results for TM polarization

Evgeni Popov*

Institute of Solid State Physics, 72 Tzarigradsko Chaussee Boulevard, 1784 Sofia, Bulgaria

Michel Nevière

Laboratoire d'Optique Electromagnétique, Faculté des Sciences et Techniques de St-Jérôme, 13397 Marseille Cedex 20, France

Received March 14, 2000; revised manuscript received June 26, 2000; accepted June 27, 2000

Using theorems of Fourier factorization, a recent paper [J. Opt. Soc. Am. A **13**, 1870 (1996)] has shown that the truncated Fourier series of products of discontinuous functions that were used in the differential theory of gratings during the past 30 years are not converging everywhere in TM polarization. They turn out to be converging everywhere only at the limit of infinitely low modulated gratings. We derive new truncated equations and implement them numerically. The computed efficiencies turn out to converge about as fast as in the TE-polarization case with respect to the number of Fourier harmonics used to represent the field. The fast convergence is observed on both metallic and dielectric gratings with sinusoidal, triangular, and lamellar profiles as well as with cylindrical and rectangular rods, and examples are shown on gratings with 100% modulation. The new formulation opens a new wide range of applications of the method, concerning not only gratings used in TM polarization but also conical diffraction, crossed gratings, three-dimensional problems, nonperiodic objects, rough surfaces, photonic band gaps, nonlinear optics, etc. The formulation also concerns the TE polarization case for a grating ruled on a magnetic material as well as gratings ruled on anisotropic materials. The method developed is applicable to any theory that requires the Fourier analysis of continuous products of discontinuous periodic functions; we propose to call it the fast Fourier factorization method.
 [S0740-3232(00)01910-4]
OCIS codes: 050.0050, 050.1940, 050.1970, 050.2770, 260.2110.

1. INTRODUCTION

Stable numerical results concerning diffraction grating efficiencies were first obtained on dielectric gratings[1,2] used as grating couplers for integrated optics at the beginning of the 1970's. When the same formalism was applied to metallic gratings used in the visible and near-infrared regions, good converging results were obtained for TE polarization, but in TM polarization a poor convergence was observed with respect to the number of spectral orders (propagating and evanescent) retained in the computation. Moreover, depending on the groove depth and the ohmic conductivity of the metal, numerical instabilities appeared above a given truncation parameter; they gave results that violated the energy-balance criterion and severely limited the use of the differential method for TM polarization and metallic gratings. These numerical difficulties had already been pointed out[3] in 1974. Since they were felt to be linked with the numerical integration process that is used in the differential theory, a lot of unpublished work was devoted to getting rid of these instabilities by changing the integration algorithm, modifying the set of equations to integrate, changing the sense of the integration process, using asymptotic expansion of the field, etc. but all the attempts turned out to be unsuccessful. Some small progress occurred in 1980 (Ref. 4) by using two simultaneous counterruning numerical integration processes, which enabled the author of Ref. 4 to analyze gratings two times deeper than those analyzed through the classical formulation. However, this improvement did not really eliminate the problem, and the differential theory of gratings was felt to be severely limited in its application range in dealing with highly reflecting metals.

This serious drawback had a happy consequence, namely, that it forced the authors of the theory to find another range of applications in which it could be useful. This new range was in the UV and x-ray spectral region[5–7]; it took many years to convince the scientific community of the necessity of requiring Maxwell equations in a spectral domain that was assumed to be free of polarization effects. Indeed, the preliminary studies done[7] in view of optimizing the recently launched x-ray–Multi-Mirror mission (XMM telescope) proved the necessity of using the electromagnetic theory at wavelengths λ as small as 0.8 nm, which led to λ/d ratios (d is groove spacing) smaller than 4×10^{-4}. Thus nowadays most synchrotron beam lines and X–UV spectroscopic missions are optimized with the differential theory of gratings. Despite this success, many years elapsed before any significant improvement occurred, and the origin of the difficulties of the differential method was not clearly understood. Some authors[8] claimed to have found the

limitation of the theory in the sense that the propagation equations that are at the basis of the theory could be false, but their arguments appeared to be wrong.[9] In fact, understanding the problem was difficult, because the numerical instabilities have two independent origins that enhance each other: (1) the numerical contamination of the results due to growing exponential functions associated with evanescent orders during the integration process and (2) the poor convergence of the Fourier series of some components of the electromagnetic field in TM polarization. Of course, the numerical contamination aggravates the slowness of the convergence of the series, while the poor convergence requires the use of larger differential sets, which aggravates the numerical contamination. The numerical contamination is not limited to the TM polarization case and metallic gratings. Indeed, it may appear even for dielectric gratings used in TE polarization, but in that case it begins to appear for a critical modulation ratio a/d (a is groove depth) close to unity, the critical value decreasing when the refractive index grows in modulus and the number of Fourier components of the field increases. This explains the fact that numerical contamination was not seen in the first studies dealing with medium modulated gratings and that it appears sooner on metallic gratings than on dielectric ones, except in the X–UV region, in which all refractive indices are close to unity. After ten years of silence, in the 1990's a great amount of work was done[10–17] to get rid of the numerical contamination that was due to growing exponential functions. Among these various approaches, the S-matrix propagation algorithm[15] seems to us the easiest one to implement. There are various ways of defining the S-matrix and the corresponding propagation algorithm, which are not strictly equivalent in terms of ease of use and stability. The way we developed the algorithm in Ref. 18 turns out to be the most stable and is particularly well suited to being coupled with the differential theory. This method has completely eliminated the first origin of the numerical problems, and it was a great satisfaction to be able to integrate fields in thick holograms along distances equal to thousands of wavelengths without seeing any divergence in the numerical results. That left only the second origin of the difficulties.

Concerning the poor convergence of the Fourier series, recent papers[19,20] proposed a reformulation of the propagation equations, which constituted great progress for lamellar profiles studied with the rigorous-coupled-wave method. But the proposed change in the equations was empirical and the origin of the improvement was not understood, and when one of the authors (M. N.) tried to use it for sinusoidal profiles studied with the differential theory, he did not see any improvement in the convergence of the Fourier series of the field. The remarkable work of Li[21] provided a solid mathematical foundation for a new formulation of the coupled-wave method. Using three theorems of Fourier factorization, Li established the extremely important following conclusion: Although the propagation equations of the original differential theory were exact—both those written in spatial variables and those in discrete Fourier space—the latter ones become ill suited as soon as they are truncated by any numerical treatment. The truncated equations no longer preserve the continuity of the appropriate field components across the discontinuities of the permittivity function. Li proposed appropriate factorization rules to preserve that continuity. In this paper we use these rules to establish new propagation equations for the differential method that can be truncated without any numerical problem. These equations are established for arbitrary profiles, of which equations given in Refs. 19 and 20 appear as particular cases. Their advantages are shown here through numerical results in various selected examples.

2. THE MATHEMATICAL PROBLEM IN THE CLASSICAL FORMULATION

The notation used in this paper follows that used in the original studies.[3,22] A grating whose profile is given by $y = f(x)$ is lighted by a TM-polarized incident plane wave of the form

$$H_z^{\,i} = A \exp[i(\alpha_0 x - \beta_0 y)],$$

which excites a total field $H_z(x, y)$ that is pseudoperiodic and is thus represented by its pseudo-Fourier series,

$$H_z(x, y) = \sum_{n=-\infty}^{+\infty} H_n(y) \exp(i\alpha_n x),$$

where $\alpha_n = \alpha_0 + nK$, $K = 2\pi/d$ and d is the groove spacing.

Inside the modulated area defined by $0 < y < a$, where a is the groove depth, the relative permittivity ϵ is periodic with respect to x. We thus introduce the periodic function $k^2(x, y) = k_0^2 \epsilon(x, y)$, where k_0 is the modulus of the wave vector in vacuum. Using Maxwell equations in the sense of distributions, the basic propagation equation for TM polarization can be established and is written as

$$\operatorname{div}\left(\frac{1}{k^2(x, y)} \overrightarrow{\operatorname{grad}}\, H_z \right) + H_z = 0. \tag{1}$$

Indeed, this equation leads to a second-order differential equation with first derivatives. Thus it is in fact transformed into a set of two coupled first-order differential equations. Let us establish these first-order differential equations directly from Maxwell equations. From Maxwell equation $\operatorname{curl}(\mathbf{H}) = -j\omega\epsilon\mathbf{E}$ and introducing $\tilde{E}_x = E_x/(j\omega\mu_0)$, $\tilde{E}_y = E_y/(j\omega\mu_0)$ (where ω is the circular frequency and μ_0 is the magnetic permittivity of vacuum), we get

$$\tilde{E}_x(x, y) = \frac{1}{k^2(x, y)} \frac{\partial H_z}{\partial y}, \tag{2}$$

$$\tilde{E}_y(x, y) = \frac{-1}{k^2(x, y)} \frac{\partial H_z}{\partial x}. \tag{3}$$

Equation (2) can be immediately inverted into

$$\frac{\partial H_z}{\partial y} = k^2(x, y)\tilde{E}_x. \tag{3'}$$

On the other hand, the Maxwell equation $\operatorname{curl}(\mathbf{E}) = j\omega\mu_0\mathbf{H}$ leads to $\partial\tilde{E}_y/\partial_x - \partial\tilde{E}_x/\partial_y = H_z$, and the use of Eq. (3) gives

$$\frac{\partial}{\partial y}\tilde{E}_x = -H_z + \frac{\partial \tilde{E}_y}{\partial x} = -H_z - \frac{\partial}{\partial x}\left(\frac{1}{k^2}\frac{\partial H_z}{\partial x}\right). \quad (4)$$

Equations (3′) and (4) are the basic equations of the differential theory of gratings. Introducing the pseudo-Fourier components H_n and $\tilde{E}_n$ of H_z and $\tilde{E}_x$ plus the Fourier components k_n^2 of k^2, we then write the equations in the Fourier space:

$$\frac{dH_n}{dy} = \sum_{m=-\infty}^{+\infty} (k^2)_{n-m}\tilde{E}_m, \quad (5)$$

$$\frac{d\tilde{E}_n}{dy} = \alpha_n \sum_{m=-\infty}^{+\infty} \alpha_m \left(\frac{1}{k^2}\right)_{n-m} H_m - H_n. \quad (6)$$

At this level the equations are still rigorous insofar as the summations over subscript m run over an infinite number of terms. But for making computations, these series have to be truncated from $-N$ to $+N$ limits, and all authors who have worked on the differential theory have assumed that such a process is valid provided that N is large enough. The great merit of the work of Li[21] was to study the legitimacy of the truncation process and to show that the equations derived from a truncation of Eqs. (5) and (6) are exact almost everywhere, but not everywhere, a fact that makes a world of difference in the computation.

Indeed, Eqs. (5) and (6) are derived from Eqs. (3′) and (4), assuming Laurent's rule, which states that the Fourier components h_n of the product $h(x)$ of two arbitrary functions $f(x)$ and $g(x)$ is simply given by

$$h_n = \sum_{m=-\infty}^{+\infty} f_{n-m} g_m.$$

To simplify the following calculations, we introduce matrix notation. We designate by $[g]$ the vector constructed with the Fourier components of $g(x)$ and by $[[f]]$ the Toeplitz matrix whose (n, m) entry is f_{n-m}. Thus the preceding equation is simply written as

$$[h] = [\![f]\!][g]. \quad (7)$$

Here both the vectors and the Toeplitz matrix have infinite size. The problem that we address is whether Eq. (7) still holds when the vectors and the Toeplitz matrix are truncated to a finite order N. The difficulty comes from the fact that, depending on the kind of discontinuities of functions $f(x)$, and $g(x)$, the truncation of Eq. (7) will, or will not, introduce errors on the reconstructed function $h(x)$ obtained through its Fourier harmonics. Li clearly derived three important conclusions[21]:

1. A product of two piecewise-smooth, bounded, periodic functions that have no concurrent jump discontinuities can be factorized by Laurent's rule:

$$h_n^{(N)} = \sum_{m=-N}^{N} f_{n-m} g_m. \quad (7')$$

2. A product of two piecewise-smooth, bounded, periodic functions that have only pairwise-complementary jump discontinuities cannot be factorized by Laurent's rule, but in most cases it can be factorized by the inverse rule:

$$h_n^{(N)} = \sum_{m=-N}^{N} \left(\left[\!\left[\frac{1}{f} \right]\!\right]^{(N)} \right)^{-1}_{n,m} g_m. \quad (8)$$

3. A product of two piecewise-smooth, bounded, periodic functions that have concurrent but not complementary jump discontinuities can be Fourier factorized neither by Laurent's rule nor by the inverse rule.

The use of the second conclusion allowed Li[21] to derive on a mathematical basis the equations previously proposed in Refs. 19 and 20 in the case of lamellar profiles. It can easily be verified that, for this simple profile, the product $k^2\tilde{E}_x$ in Eq. (3′) is continuous, since it is proportional to the component of D normal to the profile; moreover, in Eq. (4), $1/k^2(\partial H_z/\partial x)$ is also continuous, since it is proportional to E_y, which is, in this case, purely tangential. Thus the inverse rule [Eq. (8)] applies for both equations. Unfortunately, for an arbitrary groove shape the two above-mentioned products are no longer continuous, and conclusion 3 applies. Our aim in this paper is to reformulate the propagation equations in such a way that conclusions 1 and 2 can be used.

3. NEW FORMULATION OF THE DIFFERENTIAL THEORY

A. Derivation of the New Differential Set

Since E_x and E_y are never continuous functions at the boundary of an arbitrary grating profile, we express these components in terms of the tangential (E_t) and the normal (E_n) component. To that end, let us introduce the unit vector $\mathbf{t}$ of the tangent at the grating profile at a point (x_1, y) as illustrated in Fig. 1. Its components are simply given by

$$t_x = \cos\theta, \qquad t_y = \sin\theta,$$

where θ is illustrated in Fig. 1 and is defined by $\tan\theta = df/dx$, $\theta \in [-\pi/2, +\pi/2]$.

Thus E_t and E_n are written as

$$E_t = \cos\theta E_x + \sin\theta E_y, \quad (9)$$

$$E_n = -\sin\theta E_x + \cos\theta E_y. \quad (10)$$

In what follows, we use the following abbreviations:

$$c = \cos\theta, \quad s = \sin\theta.$$

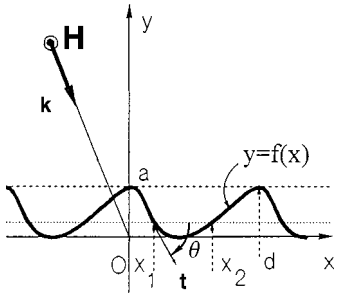

Fig. 1. Grating geometry and notation.

Thus, inverting Eqs. (9) and (10) leads to

$$\tilde{E}_x = c\tilde{E}_t - s\tilde{E}_n, \tag{11}$$

$$E_y = sE_t + cE_n, \tag{12}$$

where the tilde means that the fields are divided by $j\omega\mu_0$.

At a given ordinate y, Eqs. (9) and (10) are valid only for two values (x_1 and x_2) of x. However, we define functions $E_t(x,y)$ and $E_n(x,y)$ through a suitable continuation of functions $c(x)$ and $s(x)$ explained in what follows. This extension makes the present theory valid not only for bare profiles but also for dielectric-coated gratings and multilayer-coated gratings.

Equation (11) will first be used to calculate the nth Fourier component of $k^2\tilde{E}_x$ in Eq. (3′):

$$k^2\tilde{E}_x = ck^2\tilde{E}_t - sk^2\tilde{E}_n. \tag{13}$$

Let us study the continuity of the different terms in Eq. (13). To that end, we extrapolate functions $c(x)$ and $s(x)$ outside points x_1 and x_2 by continuous functions of x (in fact, it suffices that c and s are continuous at the points where E_x, E_y and k^2 are discontinuous). In Eq. (13) the first term on the right-hand side includes the product of the discontinuous function k^2 by a continuous function $\tilde{E}_t$. Following conclusion 1 of Li, the Fourier component of the product can be found through Laurent's rule. Concerning the second term, the product $k^2\tilde{E}_n$ is continuous, while k^2 and $\tilde{E}_n$ are discontinuous; thus the calculation of the Fourier components of the product requires the use of conclusion 2, i.e., the use of inverse rule (8). We then get

$$[k^2\tilde{E}_x] = [\![c]\!][\![k^2]\!][\tilde{E}_t] - [\![s]\!][\![1/k^2]\!]^{-1}[\tilde{E}_n]. \tag{14}$$

Analysis of the continuity of the terms appearing on the right-hand side of Eq. (9) shows that the Fourier components of $\tilde{E}_t$ can be computed through Laurent's rule:

$$[\tilde{E}_t] = [\![c]\!][\tilde{E}_x] + [\![s]\!][\tilde{E}_y]. \tag{15}$$

In a similar way, Eq. (10) gives

$$[\tilde{E}_n] = -[\![s]\!][\tilde{E}_x] + [\![c]\!][\tilde{E}_y]. \tag{16}$$

Equations (15) and (16) put into Eq. (14) lead to

$$[k^2\tilde{E}_x] = ([\![c]\!][\![k^2]\!][\![c]\!] + [\![s]\!][\![1/k^2]\!]^{-1}[\![s]\!])[\tilde{E}_x] + \left([\![c]\!][\![k^2]\!][\![s]\!] - [\![s]\!]\left[\!\left[1/k^2\right]\!\right]^{-1}[\![c]\!]\right)[\tilde{E}_y]. \tag{14′}$$

At this level, one may wonder about the commutativity of the various matrix products that appear in this equation. The commutativity of the infinite Toeplitz matrices, established in Appendix A, cannot be used on truncated matrices. Moreover, the inverse of the Toeplitz matrix $[\![1/k^2]\!]$ is not a Toeplitz one. If we were dealing with infinite matrices, we would have $[\![1/k^2]\!]^{-1} = [\![k^2]\!]$, the commutativity would hold for all products, and the multiplicative factor of $[\tilde{E}_y]$ in Eq. (14′) would vanish. This is true except at the two ends of the main diagonal of the matrix $[\![k^2]\!]$; see (Ref. 21, p. 1876). Concerning the multiplicative factor of $[\tilde{E}_x]$, we would have $[\![c]\!][\![c]\!] = [\![c^2]\!]$, $[\![s]\!][\![s]\!] = [\![s^2]\!]$, and $[\![c^2]\!] + [\![s^2]\!] = \mathbb{1}$, unit matrix. Thus Eq. (14′) would reduce to

$$[k^2\tilde{E}_x] = [\![k^2]\!][\tilde{E}_x],$$

which is merely Laurent's rule. The more complicated form of Eq. (14′) comes from the fact that for truncated matrices, some previous simplifications do not hold. However, we can put Eq. (14′) into a simpler form by working on Eq. (13) in a different way. Let us write it as

$$k^2\tilde{E}_x = k^2c\tilde{E}_t - k^2s\tilde{E}_n,$$

which implies that

$$[k^2\tilde{E}_x] = [\![k^2]\!][c\tilde{E}_t] - [\![1/k^2]\!]^{-1}[s\tilde{E}_n].$$

Using Eqs. (9) and (10), we get

$$[k^2\tilde{E}_x] = [\![k^2]\!][c^2\tilde{E}_x + cs\tilde{E}_y] + [\![1/k^2]\!]^{-1}[s^2\tilde{E}_x - cs\tilde{E}_y],$$

and the use of Laurent's rule leads to

$$[k^2\tilde{E}_x] = ([\![k^2]\!][\![c^2]\!] + [\![1/k^2]\!]^{-1}[\![s^2]\!])[\tilde{E}_x] + ([\![k^2]\!] - [\![1/k^2]\!]^{-1})[\![cs]\!][\tilde{E}_y].$$

Let us introduce matrices Δ, A, and B given by

$$\Delta = ([\![k^2]\!] - [\![1/k^2]\!]^{-1}), \qquad A = \Delta[\![c^2]\!], \qquad B = \Delta[\![cs]\!].$$

We finally obtain

$$[k^2\tilde{E}_x] = (A + [\![1/k^2]\!]^{-1})[\tilde{E}_x] + B[\tilde{E}_y]. \tag{17}$$

Then Maxwell equation (3) leads to

$$[k^2\tilde{E}_x] = \left(A + \left[\!\left[\frac{1}{k^2}\right]\!\right]^{-1}\right)[\tilde{E}_x] + B\left[-\frac{1}{k^2}\frac{\partial H_z}{\partial x}\right]. \tag{17′}$$

Here we arrive at the second key step of the theory. Between the last brackets of Eq. (17′), the product $-1/k^2(\partial H_z/\partial x)$ is discontinuous for any arbitrary grating profile, since it is equal to E_y. Moreover, both $1/k^2$ and $\partial H_z/\partial x$ are discontinuous at x_1 and x_2. Thus the Fourier components of the product can be obtained neither through Laurent's rule nor through the inverse rule. In order to derive them, we calculate the Fourier components of k^2E_y along the same lines as for $k^2\tilde{E}_x$. From Eq. (12) we have

$$k^2E_y = k^2sE_t + k^2cE_n,$$

and the study of the continuity of the different products gives

$$[k^2E_y] = [\![k^2]\!][sE_t] + [\![1/k^2]\!]^{-1}[cE_n].$$

Introducing Eqs. (9) and (10), we get

$$[k^2E_y] = [\![k^2]\!][csE_x + s^2E_y] + [\![1/k^2]\!]^{-1}[-csE_x + c^2E_y].$$

Thus

$$[k^2E_y] = [\![k^2]\!]([\![cs]\!][E_x] + [\![s^2]\!][E_y]) + [\![1/k^2]\!]^{-1} \times (-[\![cs]\!][E_x] + [\![c^2]\!][E_y]),$$

$$[k^2E_y] = B[E_x] + ([\![k^2]\!] - A)[E_y].$$

From this equation we deduce that

$$[E_y] = ([\![k^2]\!] - A)^{-1}([k^2E_y] - B[E_x]), \tag{18}$$

or

$$\left[\frac{1}{k^2}\frac{\partial H_z}{\partial x}\right] = ([\![k^2]\!] - A)^{-1}(i\alpha[H_z] + B[\tilde{E}_x]), \tag{18′}$$

where α is a diagonal matrix with elements α_n.

The use of Eqs. (3′), (17′), and (18′) leads to the first basic equation of the differential theory, and Eqs. (4) and (18′) lead to the second one:

$$\left[\frac{\partial H_z}{\partial y}\right] = (A + [\![1/k^2]\!]^{-1} - B([\![k^2]\!] - A)^{-1}B)[\tilde{E}_x] - B([\![k^2]\!]-A)^{-1} i\alpha[H_z], \tag{19}$$

$$\left[\frac{\partial \tilde{E}_x}{\partial y}\right] = \alpha([\![k^2]\!] - A)^{-1}\alpha[H_z] - [H_z] - i\alpha([\![k^2]\!] - A)^{-1}B[\tilde{E}_x]. \tag{20}$$

B. Discussion of the New Equations

Despite their apparent complexity, Eqs. (19) and (20) allow us to discuss and explain several important points.

First, if we do not truncate the Fourier series of the field ($N \to \infty$), matrix Δ is null and so are matrices A and B. Most of the terms in Eqs. (19) and (20) vanish, and the equations reduce to Eqs. (5) and (6). We then conclude that the original untruncated equations written in the Fourier space were rigorous. The problems that occurred were due to truncation only.

Second, if the modulation ratio a/d of the grating tend toward zero, $\theta \to 0$. Thus $c \to 1$, $s \to 0$, which leads to $A = \Delta$ and $B = 0$. Equations (19) and (20) reduce to

$$\left[\frac{\partial H_z}{\partial y}\right] = [\![k^2]\!][\tilde{E}_x], \tag{5′}$$

$$\left[\frac{\partial \tilde{E}_x}{\partial y}\right] = \alpha\left[\!\!\left[\frac{1}{k^2}\right]\!\!\right]\alpha[H_z] - [H_z]. \tag{6′}$$

Equations (5′) and (6′) are the truncated form of Eqs. (5) and (6). This shows that the original truncated equations in the Fourier space are exact only at the limit $a/d \to 0$. It explains why, even on highly reflecting metals, a good convergence was obtained provided that the modulation was low enough. We always observed that the higher the modulus of the permittivity of the metal, the smaller the groove depth we could analyze numerically with the original differential method. This comes from the fact that the elements of A and B increase with $|\epsilon|$, where ϵ is the permittivity of the grating material. Thus the additional terms in Eqs. (19) and (20) that were neglected in Eqs. (5′) and (6′) play an increasing role when $s \neq 0$.

Third, if $\epsilon \to 1 + i0.$, as occurs for all materials in the x-ray region, the discontinuity of ϵ between space and the grating material tends to zero. Thus all discontinuity problems vanish and all Fourier components of products can be factorized by Laurent's rule (7′). Indeed, it is easy to verify that in that case $A \to 0$, $B \to 0$, since $[\![1/k^2]\!]^{-1} \to [\![k^2]\!]$. We understand why Eqs. (5′) and (6′), which have been used to study x-ray gratings for many years, turned out to be a reliable tool in that region. The convergence of the Fourier series of the field in TM polarization was about as good as for the TE case, even under circumstances in which results depart strongly from scalar theory predictions, as occurs for gratings used under high incidence.

Fourth, what happens for a lamellar profile? In that case, for any ordinate y during the integration process, $\theta = \pi/2$, and thus $c = 0$, $s = 1$, $A = 0$, $B = 0$. Equations (19) and (20) reduce to

$$\left[\frac{\partial H_z}{\partial y}\right] = \left[\!\!\left[\frac{1}{k^2}\right]\!\!\right]^{-1}[\tilde{E}_x], \tag{21}$$

$$\left[\frac{\partial \tilde{E}_x}{\partial y}\right] = \alpha[\![k^2]\!]^{-1}\alpha[H_z] - [H_z]. \tag{22}$$

These equations are identical to Eqs. (5′) and (6′) except that $[\![k^2]\!]$ is replaced by $[\![1/k^2]\!]^{-1}$ and $[\![1/k^2]\!]$ by $[\![k^2]\!]^{-1}$. These are exactly the transformations that were proposed by the authors of Refs. 19 and 20, which resulted in a great improvement in the convergence of the Fourier series of the field for a lamellar grating. We are now in a position to understand why, when we tried to use Eqs. (21) and (22) to improve the convergence of the results on a sinusoidal profile two years ago, we obtained no improvement. Indeed, for an arbitrary profile, Eqs. (21) and (22) are as far from the exact Eqs. (19) and (20) as Eqs. (5′) and (6′) are, and the concluding remark of Ref. 19 that claimed that the numerical approach that used Eqs. (21) and (22) can be applied to any numerical techniques using Fourier expansion is not stated. The same remark applies to a similar affirmation done in Ref. 21 (p. 1875). Moreover, we explain why Lalanne found that in the small depth limit,[23] the conventional formulation of the differential theory is better conditioned than his new formulation, since at the limit the first one is rigorous.

The last point that the present work allows us to understand is the following one. Many researchers have argued that the poor convergence rate obtained with the original differential method was inherent in the TM polarization case, since we then represent by a Fourier series a function that is continuous across the grating profile but has a normal derivative discontinuous. On the other hand, for TE polarization both the field and its normal derivative are continuous. The difference in rate of convergence should be linked with the difference in regularity of the unknown functions. This explanation was in contradiction to the fact that when perfectly conducting gratings were analyzed through the differential theory after a conformal mapping,[24] no slow convergence was observed for TM polarization, although the difficulty should be expected to be stronger than for real metals. We now know that the slow convergence was not inherent in the case of polarization but was linked primarily with the way in which the differential equations were truncated in the original theory. The conformal mapping technique[24] uses other equations that are not concerned with conclusion 2 of Li.[21]

4. NUMERICAL RESULTS

The method has been implemented numerically and tried on various profiles, for both dielectric and metallic gratings. In order to appreciate the convergence of the results, we compare them with those obtained through the integral formalism[25] that was used with a number of discretization points—and terms in the kernel of the integral

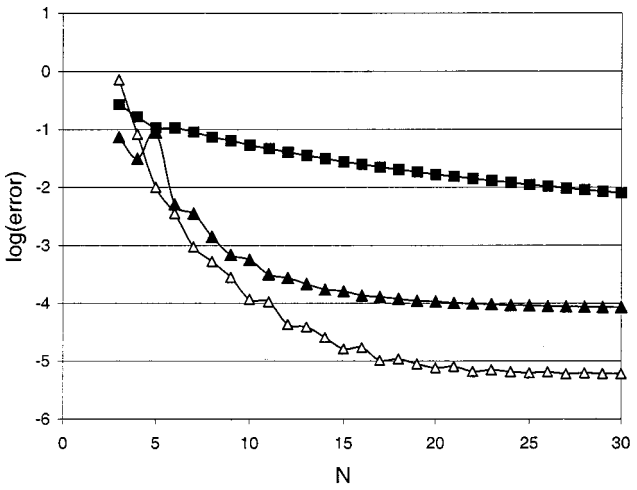

Fig. 2. Convergence of the previous and new versions of the differential theory for the case of a dielectric lamellar grating with high contrast. Squares, old version of the differential theory for TM polarization; open triangles, new version, TM polarization; solid triangles, TE polarization.

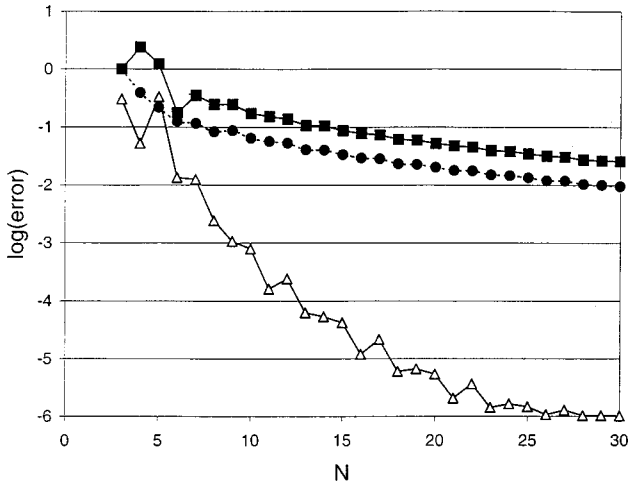

Fig. 3. Convergence of the previous and new versions of the differential theory, and the Lalanne and Morris[19] equations for a slanted (45°) lamellar grating. The grating material is the same as in Fig. 2. Solid circles are obtained with Eqs. (21) and (22).

equations—high enough to have results stabilized to better than the fifth digit. What is called the error in the following is calculated by comparison with that reference.

Figure 2 shows the results for a lamellar dielectric grating with high contrast; the modulation ratio a/d is equal to unity, the fill-in ratio is 0.4, and the refractive index is 2.5. The period d is 1 μm. It is lighted under 30° incidence angle by a 0.6328-μm wavelength. Figure 2 plots the logarithm of the relative mean square error as a function of parameter N that defines the truncation, the total number of the propagating and evanescent orders being $2N + 1$. The error is defined as

$$\frac{1}{N_p}\sum_{n=1}^{N_p}\left(\frac{\eta_n - \tilde{\eta}_n}{\eta_n}\right)^2,$$

with N_p the number of propagating orders, η_n the exact efficiency in the nth propagating order computed with a code based on the integral theory,[25] and $\tilde{\eta}_n$ the corresponding efficiency computed through the methods for which we tested the convergence.

The squares are obtained by using Eqs. (5′) and (6′), and the open triangles are obtained by using Eqs. (19) and (20), which in this case reduce to Eqs. (21) and (22). As previously observed by Lalanne and Morris,[19] a strong improvement is obtained, an error of 10^{-4} being reached with $N \approx 10$, i.e., 21 Fourier components of the field. In that case, the convergence obtained with the new method is even a little faster than the one obtained in TE polarization, shown by solid triangles.

Of course, our basic equations (19) and (20) differ significantly from those of Lalanne when $c \neq 0$, as illustrated in Fig. 3. Here we deal with a slanted lamellar grating (also called a parallelogrammic grating), with a slant angle of 45°. All other parameters are the same as in Fig. 2 except the modulation a/d, which is equal to 0.6. As observed, the convergence of Eqs. (21) and (22) is almost as bad as for the classical differential method. In contrast, with the more general equations (19) and (20), which take into account that both c and s are not null, the convergence is much faster. It is worth noting that a value close to -6 for the logarithm of the error is a very good result since it means that among the N_p propagating orders, no order is computed with a *relative* error greater than 10^{-3} N_p.

Let us move now to a deep sinusoidal profile with high contrast. Deep sinusoidal profiles and cylindrical rod gratings are the most difficult cases to compute, because the tangential-to-the-profile vector changes its direction from parallel to the x axis [for which the classical formulation in Eqs. (5′) and (6′) holds] to parallel to the y axis [for which the Lalanne formulation in Eqs. (21) and (22) is rigorous] through all intermediate cases for which Eqs. (19) and (20) apply. Moreover, the determination of the matrix Δ has to be done at each step of the integration. In contrast, according to the choice of c^2 and cs presented in Appendix B, their Fourier transform is done once for the entire integration process. Figure 4 shows the error obtained on a sinusoidal profile with the same optogeometrical parameters as in Fig. 2. The superiority of the new formulation over the previous one is evident, an error close to 10^{-4} being approached with $N = 8$ (17 spectral

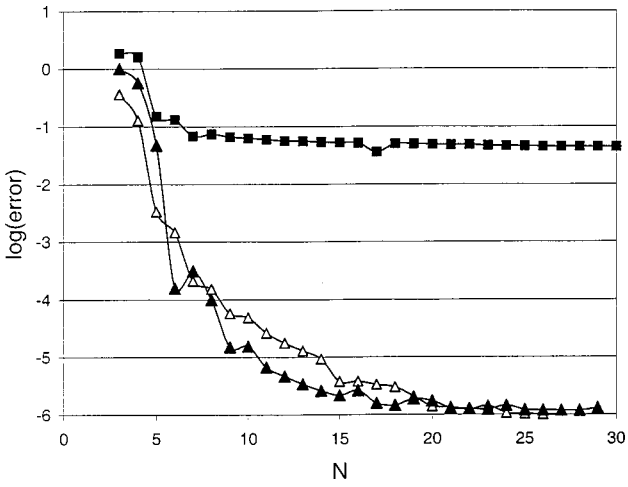

Fig. 4. Same as in Fig. 2, but for a sinusoidal profile.

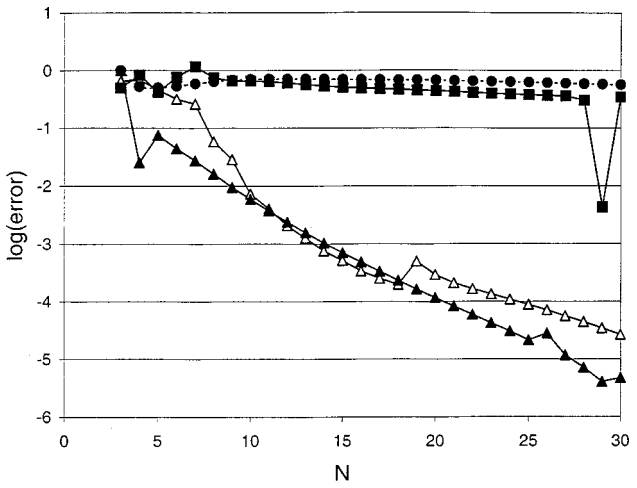

Fig. 5. Same as in Fig. 2, but for an aluminum sinusoidal profile. The solid circles are obtained with Eqs. (21) and (22).

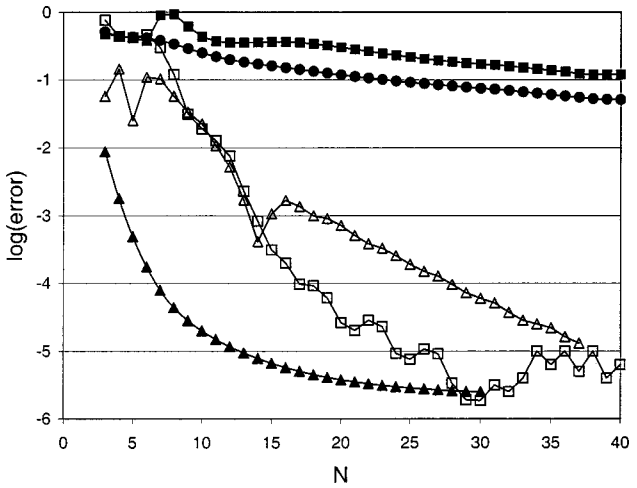

Fig. 6. Same as in Fig. 5, but for a triangular (echelette) profile with 30° blaze angle, 90° apex angle.

orders), which is very similar to the convergence rate of TE polarization. Concerning the computation time, comparisons were done on a personal computer, with four sublayers used in the S-matrix propagation algorithm and 100 integration steps in each sublayer. With $N = 10\,(a/d = 1)$ the computation time is 1.6 s in TE polarization, 3.9 s in TM polarization analyzed with the classical (previous) formulation, and 7.6 s in TM polarization analyzed with the present formulation. The ratio close to 2 between the two formulation computation times is negligible when one considers the gain of time resulting from the faster convergence of the Fourier series, which, first, reduces the computation time as N^3 and, second, reduces the number of slices in the S-matrix propagation algorithm.

In Fig. 5 we still deal with the deep sinusoidal grating, but a good reflecting metal, namely, aluminum with refractive index $1.3 + i7.6$, replaces the high-index dielectric. As expected (and previously observed two years ago), the formulation given by Eqs. (21) and (22) does not bring any improvement in that case; it is even a little worse than the classical one. On the other hand, the new formulation leads to an error lower than 10^{-4} when $N > 24$. The result is quite interesting for such a difficult grating problem and leads to very reasonable computation times. Similar results are presented on an echelette (triangular) grating with 30° blaze angle, 90° apex angle in Fig. 6. The groove spacing, wavelength, and incidence as well as the grating material are the same as in Fig. 5. An error less than 10^{-4} is obtained for $N = 27$, i.e., 55 Fourier components, while both Eqs. (5′), (6′), and (21), (22) do not converge. A better convergence is even obtained (open squares) by writing the equations as suggested at the end of Section 1 of Appendix B.

In order to convince the reader of the potential of the new formulation, we analyze numerically an effect that was recently published[26] and that has attracted a great amount of interest in the scientific community. We consider a rectangular rod grating. The rods are made with silver. The groove spacing is 0.9 μm, the groove height is 0.2 μm, and the groove width is 0.02 μm. The rods lie on a glass substrate with refractive index 1.44. The grating is lighted under normal incidence, and Fig. 7 plots the

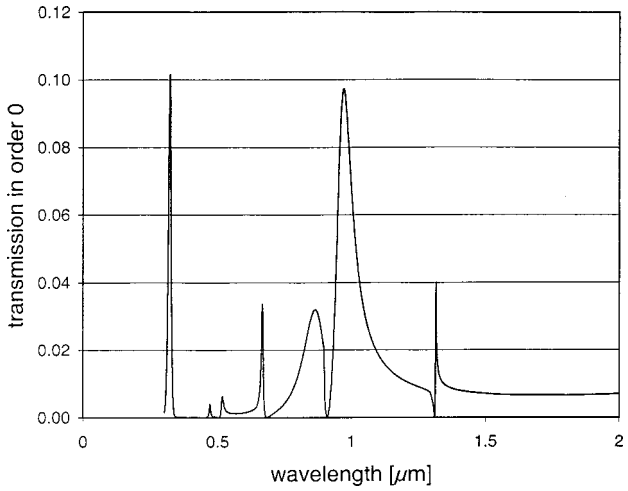

Fig. 7. Zero-order transmitted efficiency of a silver rectangular rod grating lying on a glass substrate, as a function of the wavelength. Filling ratio 0.978.

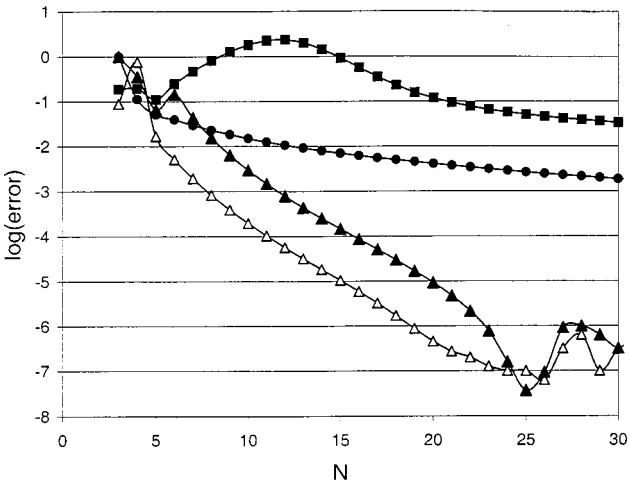

Fig. 8. Same as in Fig. 2, but for a cylindrical rod grating, $r = d/2$; solid circles are obtained with Eqs. (21) and (22). The continuation of ε^2 is made according to Eq. (B5).

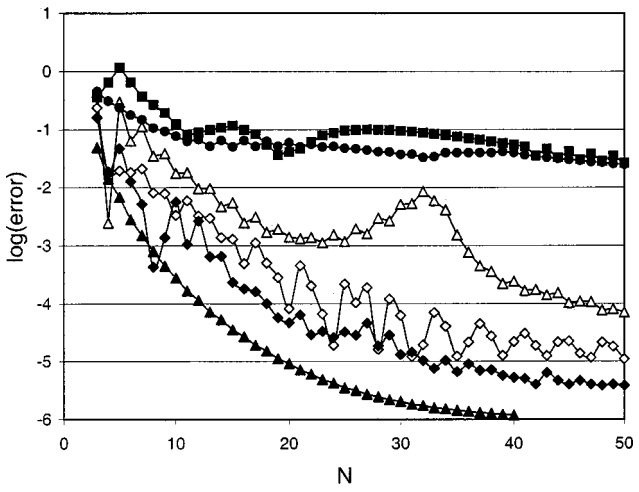

Fig. 9. Same as in Fig. 8, but for a metallic rod, $r = d/4$. Open triangles, continuation of c^2 according to Eq. (B5); diamonds, continuation of c^2 according to Eqs. (B7).

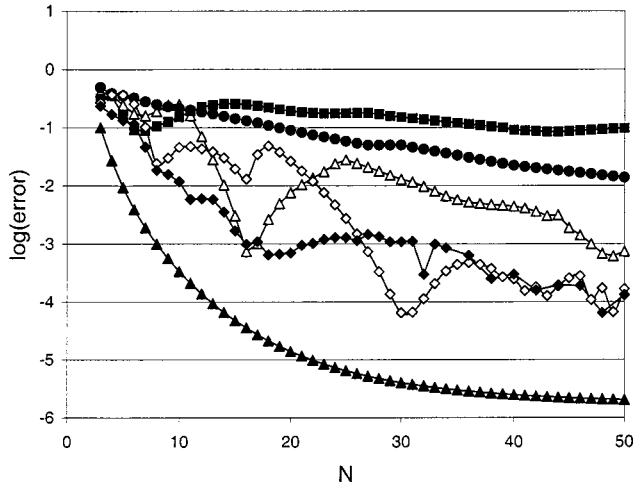

Fig. 10. Same as in Fig. 9, but for $r = d/2$.

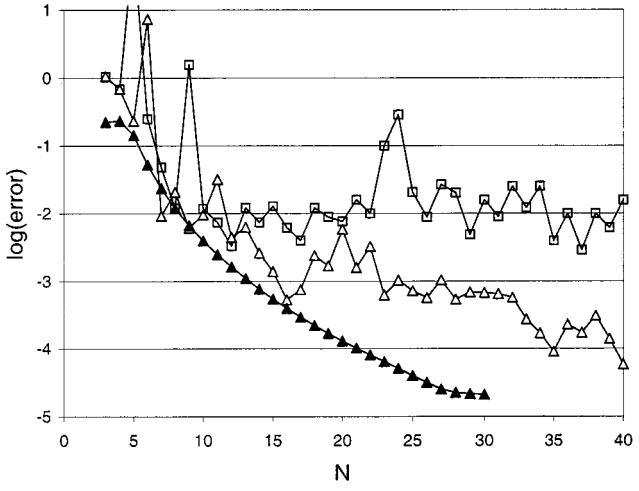

Fig. 11. Convergence of the method on a highly conducting sinusoidal grating; refractive index 0.1 + i20.

zero-order transmitted intensity as a function of wavelength. The groove width of 0.02 μm corresponds to a filling ratio of 0.978, the same as for the two-dimensional grating consisting of small cylindrical holes in a metallic sheet.[26] Although our analysis relies on a one-dimensional model of the phenomenon described in Ref. 26, the expected extraordinary transmission through subwavelength hole arrays is found as well as the expected peaks due to surface plasmons. Such a curve could not have been obtained with the previous differential methods.

Another interesting example is given in Fig. 8, which shows the convergence rate of the transmission spectrum obtained with a periodic array of cylindrical, dielectric rods. The groove spacing is 1 μm, the radius r of the rods is 0.5 μm, and their refractive index is 2.5. They are lying in vacuum and lighted under 30° incidence. This case involves the most complicated geometry, in the sense that during the integration process the tangential unit vector varies from horizontal to vertical position. However, Eqs. (19) and (20) correctly handle the situation; thus the new formulation has good potential for studying two-dimensional photonic crystals. When the dielectric rods are replaced by metallic ones, the convergence rate is preserved for a rod radius of 0.25 μm (i.e., $a/d = 0.5$) (Fig. 9); however, better convergence (diamonds) is observed when the functions cs and c^2 are recalculated at each step of the integration process, as discussed in Appendix B [Eqs. (B7) instead of Eq. (B5)]. When the cylinders touch each other ($r = d/2$, i.e., $a/d = 1$), for metallic rods a slightly less rapid convergence is observed (Fig. 10), independent of the choice of the continuation of cs and c^2.

Concerning the performance of the method on highly conducting metals, Fig. 11 shows the results obtained with a 50% modulated sinusoidal grating ($a/d = 0.5$) made of a metal with refractive index equal to 0.1 + i20. It illustrates the noncommutativity of the truncated matrices that appear in our equations. The results obtained by the classical differential method are presented only for TE polarization, because of the complete failure of the method in TM polarization. The squares were obtained assuming the commutativity of matrix Δ on the one hand and matrices $[[c^2]]$ and $[cs]$ on the other hand, as assumed in our recent previous paper.[27] The open triangles were obtained with Eqs. (19) and (20). With $N = 24$, i.e., 49 Fourier components, the diffraction problem is accurately resolved with the present work, whereas it is not so with our previous work, which does not yet converge. This numerically verifies the noncommutativity of the matrices. However, they commute in the nontruncated limit. Numerical experience not presented here shows that the different formulations presented here and in Ref. 27 give almost identical results on dielectric gratings and on aluminum gratings with not-so-high reflectivity. However, Fig. 11 shows that the present formulation is preferable, insofar as the grating profile has no wedge, so that functions $c(x)$ and $s(x)$ are continuous everywhere.

5. CONCLUSION

The beautiful work of Li[21] has provided the mathematical basis that was necessary to clarify and eliminate the last remaining difficulty inherent in the differential theory of

gratings. We now know that the poor convergence of the Fourier series of the field was not inherent in the case of TM polarization but was linked with the truncation of the propagation equations that, in the original formulation, led to a convergence almost everywhere. The new formulation leads to a convergence everywhere, and although both formulations are rigorous at the limit of infinite series, a great difference appears at the numerical level.

For the sake of clarity, we have presented only the equations for TM polarization and bare gratings. But our work is not limited to that case, and the present method can also be applied to dielectric-coated and multilayer-coated gratings. The method that we have used to obtain the basic equations (19) and (20) can also be used to reformulate the differential theory for conical diffraction,[22,28] crossed gratings,[29,30] and, more generally, three-dimensional objects. It is concerned with any numerical work in science that requires Fourier factorization of the continuous product of discontinuous functions, so we propose to call it the fast Fourier factorization method. Its consequences for the broad field of nonlinear optics are immediate. In that field, many sophisticated theories[31] have been developed owing to the fact that the differential theory was not converging in a satisfactory way, a substantial effort that could have been saved by the present work. The fast Fourier factorization method will also benefit the rapidly developing domain of photonic crystals.[32] Indeed, this work will benefit many researchers and engineers, since the differential theory of gratings is the easiest one to teach. In contrast to the other grating theories,[33] which require sophisticated mathematics, teaching the differential theory requires only the knowledge of partial derivatives, Fourier series, and matrix algebra. Thus it can be taught to undergraduate students. It is a great satisfaction to have arrived at the present result after a quarter of century of effort.

APPENDIX A: COMMUTATIVITY OF THE INFINITE TOEPLITZ MATRICES CONSTRUCTED WITH FOURIER COMPONENTS OF PERIODIC FUNCTIONS

We illustrate the commutativity on the example of the product $[\![k^2]\!][\![c]\!]$, where both matrices have infinite dimensions.

Let us consider

$$e = [\![c]\!][\![k^2]\!],$$

whose (n, m) entry is given by

$$e_{n,m} = \sum_{p=-\infty}^{+\infty} c_{n-p}(k^2)_{p-m}.$$

Thus

$$e_{n,m} = \sum_{p=-\infty}^{+\infty} c_{n-m-(p-m)}(k^2)_{p-m}. \tag{A1}$$

Defining $p' = p - m$, we obtain

$$e_{n,m} = \sum_{p'=-\infty}^{+\infty} c_{n-m-p'}(k^2)_{p'}. \tag{A2}$$

Let us now consider the nth Fourier component g_n of the product $k^2(x)c(x)$, which is equal to $c(x)k^2(x)$. We thus have

$$g_n = \sum_{r=-\infty}^{+\infty} k^2_{n-r}c_r = \sum_{s=-\infty}^{+\infty} c_{n-s}(k^2)_s.$$

Thus Eq. (A2) can be changed into

$$e_{n,m} = \sum_{r=-\infty}^{+\infty} (k^2)_{n-m-r}c_r.$$

Defining $t = r + m$, from which $r = t - m$, we obtain

$$e_{n,m} = \sum_{t=-\infty}^{+\infty} (k^2)_{n-m-t+m}c_{t-m} = \sum_{t=-\infty}^{+\infty} (k^2)_{n-t}c_{t-m}.$$

The latter expression is the (n, m) entry of the product $[\![k^2]\!][\![c]\!]$, which establishes the commutativity.

The commutativity holds for all Toeplitz matrices such as $[\![k^2]\!]$, $[\![c]\!]$, $[\![s]\!]$, constructed with the Fourier components of a periodic function, provided that the matrices are infinite. The transformation from Eq. (A1) to Eq. (A2) cannot be done for truncated matrices, and the demonstration no longer holds. Moreover, it is easy to understand that when we work on truncated matrices, it is better, for convergence purposes, to write the various products with the Toeplitz matrices of discontinuous quantities on the left. If, for example, k^2 is discontinuous while c is continuous, we have

$$[k^2c]^{(N)} = [\![k^2]\!][c] = \sum_{m=-N}^{+N} k^2_{n-m}c_m, \tag{A3}$$

$$[k^2c]^{(N)} = [ck^2]^{(N)} = [\![c]\!][k^2] = \sum_{m=-N}^{+N} c_{n-m}k^2_m. \tag{A4}$$

Equation (A3) makes use of $2N + 1$ Fourier components c_m and $2(2N + 1) - 1$ Fourier components of k^2, whereas it is the reverse for Eq. (A4). Since the Fourier components of a continuous function decrease as $1/m^2$ whereas those of a discontinuous function decrease as $1/m$, when $m \to \infty$, Eq. (A4) more severely truncates the Fourier series, which decreases more slowly. Thus Eq. (A3) is preferable. This simple observation is used to obtain Eqs. (17) and (18).

APPENDIX B: CALCULATION OF TOEPLITZ MATRICES $[\![c^2]\!]$ AND $[\![cs]\!]$

This appendix explains how to calculate the Toeplitz matrices $[\![c^2]\!]$ and $[\![cs]\!]$ for various common grating profiles. The simplest case of lamellar profile, which leads to Eqs. (21) and (22) will not be addressed here.

The quantities c and s are defined only at points x_1 and x_2, while Eqs. (11) and (12) have to be valid at any abscissa x. This requires the definition of functions $c(x)$

and $s(x)$ that take the correct values c and s at x_1 and x_2 and verify that $c^2 + s^2 = 1$, $\forall x$. This condition, which is obvious on the grating profile, is not so evident outside it. We have to remember that c and s are the components of a unit vector **t**, which was used to define the coordinate transformation in Eqs. (9), (10) or (11), (12). In these equations we choose to preserve the metrics [otherwise elements of a metric tensor would appear in Eqs. (9)–(12)], so **t** must remain a unit vector everywhere; thus $c^2 + s^2 = 1$, $\forall x$. Failure to do so would result in E_t and E_n components such that ${E_t}^2 + {E_n}^2 \neq E^2$. Moreover, in obtaining Eqs. (17) we have made use of the relation $[\![s]\!]^2 = \mathbb{1} - [\![c^2]\!]$.

The continuation of functions $c(x)$ and $s(x)$ should be done in such a way that functions are obtained that are continuous at the discontinuities x_1 and x_2 of $k^2(x, y)$. In what follows, we stick to these rules in defining $c^2(x)$ and $c(x)s(x)$ for different profiles. When possible, c^2 and cs are chosen to be continuous functions $\forall x$ in order to ensure faster convergence of their Fourier series. Of course, our choices are not the only possible ones, but it is worth noting that any time the grating profile is given by a function $y = f(x)$, our choices make the theory utilizable for multilayer-coated gratings.

1. Triangular Profile

The triangular profile is illustrated in Fig. 12, which introduces some new notation. The blaze angle is θ, and the second base angle θ_B (θ, $\theta_B > 0$). For any ordinate y during the integration process, we have

$$\text{at point } (x_1, y): \quad c = \cos\theta_B, \quad s = -\sin\theta_B,$$

$$\text{at point } (x_2, y): \quad c = \cos\theta, \quad s = \sin\theta.$$

We recall that in order to Fourier analyze with respect to x the functions c and s, which are defined only at points x_1 and x_2, we have to extend their definition over the entire period d. This can be done in any conventional way, by using a continuous or a discontinuous continuation. The only important point to remember is that for use of the inverse rule to be allowed, the continued function must be continuous at the discontinuity points of $k^2(x, y)$ (i.e., at x_1 and x_2), while it may be discontinuous anywhere else. Since c and s take two different values at x_1 and x_2, we propose to choose as continuation the following step functions:

$$c(x) = \cos\theta_B, \quad \forall x \in [0, b], \tag{B1}$$

$$= \cos\theta, \quad \forall x \in]b, d],$$

$$s(x) = -\sin\theta_B, \quad \forall x \in [0, b],$$

$$= \sin\theta, \quad \forall x \in]b, d]. \tag{B2}$$

We note that for $y = 0$, $x_1 = b = x_2$, but since the profile has no plateau, the function $k^2(x, 0)$ is continuous. Thus no problem occurs in calculating the Fourier components of $k^2(x, 0)c^2$ or $k^2(x, 0)cs$, since conclusion 1 of Li[21] still applies.

The Fourier components of the step functions c^2 and cs are then determined only once for the entire integration process by the standard fast Fourier transform method, from which we construct the Toeplitz matrices $[\![c^2]\!]$ and $[\![cs]\!]$. We note, however, that since $c(x)$ and $s(x)$ are discontinuous at $x = b$, the remark made at the end of Appendix A does not apply. Other ways of writing the matrix products, e.g., the one presented in Ref. 27, may give a convergence slightly faster than the one obtained with Eqs. (19) and (20).

2. Trapezoidal Profile

The trapezoidal profile is a triangular one truncated at top and bottom (Fig. 13); thus c and s have the same values as in the previous section. Care must be taken when we choose the discontinuity point of their extension, since now for $y = 0$, $x_1 = b$, where $k^2(x, 0)$ is discontinuous. We thus can replace b in Eqs. (B1) and (B2) with any abscissa l between b and b', the extremities of the lower plateau.

Thus $c(x)$ and $s(x)$ are written as

$$c(x) = \cos\theta_B \quad \forall x \in [0, l],$$

$$= \cos\theta, \quad \forall x \in [l, d], \tag{B3}$$

$$s(x) = -\sin\theta_B, \quad \forall x \in]0, l],$$

$$= \sin\theta, \quad \forall x \in]l, d]. \tag{B4}$$

Numerical results have shown that the convergence rate does not significantly depend on the choice of l between b and b'.

3. Sinusoidal Profile

The sinusoidal profile is given by $y = f(x) \equiv (a/2)(1 + \cos Kx)$, $K = 2\pi/d$. Using the definition of θ illustrated in Fig. 1, we obtain

$$\tan\theta = \frac{df}{dx} = -\frac{\pi a}{d}\sin Kx.$$

Then

$$c(x_1) = \frac{1}{(1 + \tan^2\theta)^{1/2}} = \frac{1}{[1 + (\pi^2 a^2)/d^2 \sin^2(Kx_1)]^{1/2}}.$$

Since $Kx_1 = \cos^{-1}(2y/a - 1)$, we get

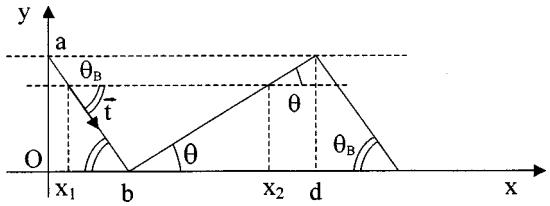

Fig. 12. Geometrical parameters of an echelette profile.

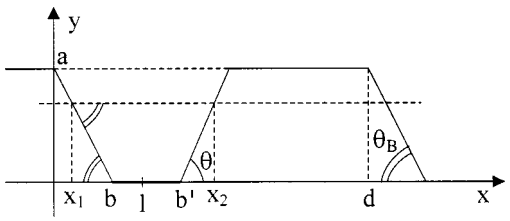

Fig. 13. Geometrical parameters of a trapezoidal profile.

$$\cos(Kx_1) = \frac{2y}{a} - 1,$$

$$\sin^2(Kx_1) = 1 - \left(\frac{2y}{a} - 1\right)^2 = \frac{4y}{a}\left(1 - \frac{y}{a}\right).$$

Finally,

$$c(x_1)\frac{1}{[1 + K^2y(a - y)]^{1/2}} \equiv c(x_2).$$

In a similar way,

$$s(x_1) = \frac{\tan\theta}{(1 + \tan^2\theta)^{1/2}} = \frac{K[y(a - y)]^{1/2}}{[1 + K^2y(a - y)]^{1/2}} = -s(x_2).$$

From these values we deduce that

$$c^2(x_1) = c^2(x_2) = \frac{1}{1 + K^2y(a - y)},$$

$$cs(x_1) = -cs(x_2) = \frac{K[y(a - y)]^{1/2}}{1 + K^2y(a - y)},$$

and these functions can be continued over the entire period in the following way.

We can choose for $c^2(x)$ a continuous function equal to

$$1/(1 + \tan^2\theta) = 1/(1 + f'^2) = 1 \Big/ \left(1 + \frac{\pi^2a^2}{d^2}\sin^2 Kx\right),$$

which gives the correct values for $x = x_1$ and $x = x_2$. For $cs(x)$ we choose the continuous function $\tan\theta/(1 + \tan^2\theta)$, equal to $f'/(1 + f'^2)$, i.e., to

$$-\frac{\pi a}{d}\sin(Kx) \Big/ \left(1 + \frac{\pi^2a^2}{d^2}\sin^2 Kx\right).$$

Such a continuation is suitable, because c^2 and cs do not depend on y, and their Fourier transform is made only once for the entire integration process.

It is interesting to note that the continuation that we proposed for triangular and trapezoidal profiles is a particular case of the present continuation, for which $\tan\theta = df/dx$ is a constant with respect to x in the intervals $[0, l]$ and $[l, d]$.

Any arbitrary profile given by a function $y = f(x)$ can be analyzed along the same lines. On the other hand, phase gratings with continuous change of refractive index along the period are not affected by the present study. They can be perfectly analyzed through the previous formulation of the differential method.

4. Cylindrical Rod Grating

The parametric equations of the central circle illustrated in Fig. 14 are written as

$$x = \frac{a}{2}\cos\phi,$$

$$y = \frac{a}{2}(1 + \sin\phi).$$

Since with the chosen orientation we have $t_x \propto -dx/d\phi$, $t_y \propto -dy/d\phi$, we get

$$c(x_1) = c(x_2) \propto \frac{a}{2}\sin\phi \propto y - \frac{a}{2},$$

$$s(x_1) = -s(x_2) \propto -[y(a - y)]^{1/2}.$$

After normalization, we finally have (taking into account that $r = a/2$)

$$c(x_1) = c(x_2) = (y - a/2) \Big/ \left[\left(y - \frac{a}{2}\right)^2 + y(a - y)\right]^{1/2} = \frac{y - r}{r},$$

$$s(x_1) = -s(x_2) = -[y(a - y)]^{1/2} \Big/ \left[\left(y - \frac{a}{2}\right)^2 + y(a - y)\right]^{1/2} = \frac{x_1}{r}.$$

As for the other profiles, there are many possible definitions of c and s for each x. We choose two of them to make a numerical test of the convergence rate. The first choice is determined so as to be independent of the vertical coordinate y, so that the Fourier transform is made only once. For values of x such that $-r < x < r$,

$$c^2(x) = 1 - x^2/r^2, \tag{B5}$$

$$cs(x) = \pm\{c^2(x)[1 - c^2(x)]\}^{1/2}. \tag{B6}$$

Outside the interval $-r < x < r$, $c^2 = cs = 0$. Although good enough for dielectric rods, this choice leads to some problems for metallic rods (see Fig. 9).

Our second choice of the way the functions are continued takes into account that the lowest (and the highest) part of the cylinder resembles a shallower sinusoidal grating, while its middle part looks like a lamellar grating. The function $c^2(x)$ is defined in the following manner:

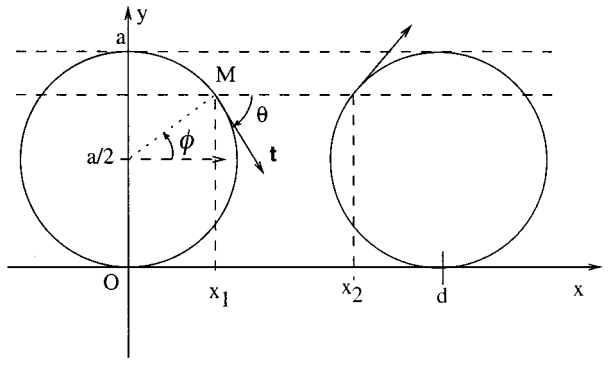

Fig. 14. Geometrical parameters of a cylindrical rod grating.

$$c^2(x) = (y - r)^2/r^2,$$
$$cs(x) = -\text{sign}(x)(y - r)[y(2r - y)]^{1/2}/r^2. \quad \text{(B7)}$$

However, in this case, $cs(x)$ has a jump at $x = 0$. It is possible to make another choice to ensure that both c^2 and cs are continuous functions of x:

$$c^2(x_1) = c^2(x_2) = (y - r)^2/r^2,$$
$$c^2(0) = c^2(d/2) = c^2(d) = \begin{cases} 1, & |y - r| > 2r/3 \\ 0, & |y - r| < 2r/3 \end{cases} \quad \text{(B8)}$$

Between the points 0, x_1, $d/2$, x_2, and d, the function $c^2(x)$ is defined by using linear interpolation. Then $cs(x)$ is determined by Eq. (B6). As observed in Figs. 9 and 10 (solid diamonds), this choice [Eq. (B8)] results in a more regular convergence than the two other choice [Eqs. (B5) and (B6), open triangles; and Eqs. (B7), open diamonds].

Corresponding author M. Nevière can be reached at the address on the title page or by e-mail, neviere@loe.univ-3mrs.fr.

*Present address, Laboratoire d'Electromagnétisme, Microondes et Optoélectronique, École Nationale Supérieure d'Electronique et de Radioélectricité de Grenoble, Institut National Polytechnique de Grenoble, 23 rue des Martyrs, BP 257, 38016 Grenoble Cedex 1, France.

REFERENCES

1. M. Nevière, R. Petit, and M. Cadilhac, "About the theory of optical grating coupler-waveguide systems," Opt. Commun. **8**, 113–117 (1973).
2. M. Nevière, P. Vincent, R. Petit, and M. Cadilhac, "Systematic study of resonances of holographic thin film couplers," Opt. Commun. **9**, 48–53 (1973).
3. M. Nevière, P. Vincent, and R. Petit, "Sur la théorie du réseau conducteur et ses applications à l'optique," Nouv. Rev. Opt. **5**, 65–77 (1974).
4. P. Vincent, "New improvement of the differential formalism for high-modulated gratings," in *Periodic Structures, Gratings, Moiré Patterns and Diffraction Phenomena*, C. H. Chi, E. G. Loewen, and C. L. O'Bryan III, eds., Proc. SPIE **240**, 147–154 (1980).
5. M. Nevière and J. Flamand, "Electromagnetic theory as it applies to X-ray and XUV gratings," Nucl. Instrum. Methods **172**, 273–279 (1980).
6. M. Nevière, J. Flamand, and J. M. Lerner, "Optimization of gratings for soft X-ray monochromators," Nucl. Instrum. Methods **195**, 183–189 (1982).
7. A. J. F. den Boggende, P. A. J. de Korte, P. H. Videler, A. C. Brinkman, S. M. Kahn, W. W. Craig, C. J. Hailey, and M. Nevière, "Efficiencies of X-ray reflection gratings," in *X-Ray Instruments, Multilayers and Sources*, J. F. Marshall, ed., Proc. SPIE **982**, 283–298 (1988).
8. R. A. Depine and J. M. Simon, "Comparison between the differential and integral methods used to solve the grating problem in the H∥ case," J. Opt. Soc. Am. A **4**, 834–838 (1987).
9. M. Nevière and P. Vincent, "Differential theory of gratings: answer to an objection on its validity for TM polarization," J. Opt. Soc. Am. A **5**, 1522–1524 (1988).
10. D. M. Pai and K. A. Awada, "Analysis of dielectric gratings of arbitrary profiles and thicknesses," J. Opt. Soc. Am. A **8**, 755–762 (1991).
11. L. Li, "Multilayer modal method for diffraction gratings of arbitrary profile, depth, and permittivity," J. Opt. Soc. Am. A **10**, 2581–2593 (1993).
12. M. Nevière and F. Montiel, "Deep gratings: a combination of the differential theory and the multiple reflection series," Opt. Commun. **108**, 1–7 (1994).
13. F. Montiel and M. Nevière, "Differential theory of gratings: extension to deep gratings of arbitrary profile and permittivity through the *R*-matrix propagation algorithm," J. Opt. Soc. Am. A **11**, 3241–3250 (1994).
14. N. Chateau and J. P. Hugonin, "Algorithm for the rigorous coupled-wave analysis of grating diffraction," J. Opt. Soc. Am. A **11**, 1321–1331 (1994).
15. L. Li, "Formulation and comparison of two recursive matrix algorithms for modeling layered diffraction gratings," J. Opt. Soc. Am. A **13**, 1024–1035 (1996).
16. M. G. Moharam, D. A. Pommet, E. B. Grann, and T. K. Gaylord, "Stable implementation of the rigorous coupled-wave analysis for surface-relief gratings: enhanced transmission matrix approach," J. Opt. Soc. Am. A **12**, 1077–1086 (1995).
17. R. H. Morf, "Exponentially convergent and numerically efficient solution of Maxwell equations for lamellar gratings," J. Opt. Soc. Am. A **12**, 1043–1056 (1995).
18. F. Montiel, M. Nevière, and P. Peyrot, "Waveguide confinement of Čerenkov second-harmonic generation through a graded-index grating coupler: electromagnetic optimization," J. Mod. Opt. **45**, 2169–2186 (1988).
19. P. Lalanne and G. M. Morris, "Highly improved convergence of the coupled-wave method for TM polarization," J. Opt. Soc. Am. A **13**, 779–784 (1996).
20. G. Granet and B. Guizal, "Efficient implementation of the coupled-wave method for metallic gratings in TM polarization," J. Opt. Soc. Am. A **13**, 1019–1023 (1996).
21. L. Li, "Use of Fourier series in the analysis of discontinuous periodic structures," J. Opt. Soc. Am. A **13**, 1870–1876 (1996).
22. P. Vincent, "Differential methods," in *Electromagnetic Theory of Gratings*, Vol. 22 of Topics in Current Physics, R. Petit ed. (Springer-Verlag, Berlin, 1980), pp. 101–121.
23. P. Lalanne, "Convergence performance of the coupled-wave and the differential method for thin gratings," J. Opt. Soc. Am. A **14**, 1583–1591 (1977).
24. M. Nevière, M. Cadilhac, and R. Petit, "Applications of conformal mappings to the diffraction of electromagnetic waves by a grating," IEEE Trans. Antennas Propag. **AP-21**, 37–46 (1973).
25. D. Maystre, "Integral methods," in *Electromagnetic Theory of Gratings*, Vol. 22 of Topics in Current Physics, R. Petit ed. (Springer-Verlag, Berlin, 1980), pp. 63–100.
26. T. W. Ebbesen, H. J. Lezec, H. F. Ghaemi, T. Thio, P. A. Wolff, "Extraordinary optical transmission through subwavelength hole arrays," Nature **391**, 667–669 (1998).
27. E. Popov and M. Nevière, "Differential theory for diffraction gratings: new formulation for TM polarization with rapid convergence," Opt. Lett. **25**, 598–600 (2000).
28. P. Vincent, M. Nevière, and D. Maystre, "Computation of the efficiencies and polarization effects of XUV gratings used in classical and conical mountings," Nucl. Instrum. Methods **152**, 123–126 (1978).
29. D. Maystre and M. Nevière, "Electromagnetic theory of crossed gratings," J. Opt. (Paris) **9**, 301–306 (1978).
30. P. Vincent, "A finite-difference method for dielectric and conducting crossed gratings," Opt. Commun. **26**, 293–296 1978.
31. M. Nevière, E. Popov, R. Reinisch, and G. Vitrant, *Electromagnetic Resonances in Nonlinear Optics* (Gordon & Breach, London, UK) (to be published).
32. P. L. Knight, ed., Special issue on Photonic Band Structures, J. Mod. Opt. **41**(2) (1994).
33. M. Nevière and E. Popov, "Grating electromagnetic theory user guide," J. Imaging Sci. Technol. **41**, 315–323 (1997).